Biochemistry

pubs.acs.org/biochemistry
Article

Periostin C-Terminal Is Intrinsically Disordered and Interacts with 143 Proteins in an In Vitro Epidermal Model of Atopic Dermatitis

Christian E. Rusbjerg-Weberskov, Mette Liere Johansen, Jan S. Nowak, Daniel E. Otzen, Jan Skov Pedersen, Jan J. Enghild,* and Nadia Sukusu Nielsen

Cite This: *Biochemistry* 2023, 62, 2803−2815

ABSTRACT: Human periostin is a 78−91 kDa matricellular protein implicated in extracellular matrix remodeling, tumor development, metastasis, and inflammatory diseases like atopic dermatitis, psoriasis, and asthma. The protein consists of six domains, including an N-terminal Cys-rich CROPT domain, four fasciclin-1 domains, and a C-terminal domain. The exons encoding the C-terminal domain may be alternatively spliced by shuffling four exons, generating ten variants of unknown function. Here, we investigate the structure and interactome of the full-length variant of the C-terminal domain with no exons spliced out. The structural analysis showed that the C-terminal domain lacked a tertiary structure and was intrinsically disordered. In addition, we show that the motif responsible for heparin-binding is in the conserved very C-terminal part of periostin. Pull-down confirmed three known interaction partners and identified an additional 140 proteins, among which nine previously have been implicated in atopic dermatitis. Based on our findings, we suggest that the C-terminal domain of periostin facilitates interactions between connective tissue components in concert with the four fasciclin domains.

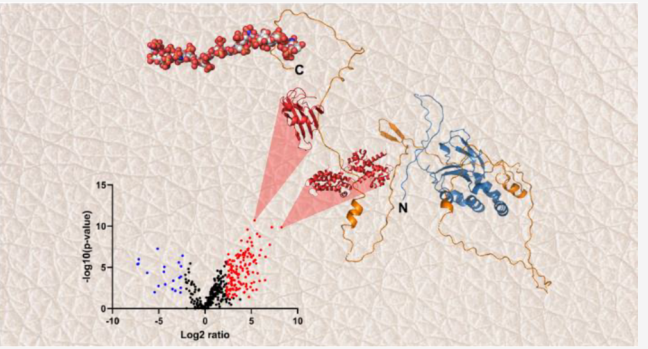

INTRODUCTION

Periostin is a matricellular protein found in connective tissues involved in extracellular matrix remodeling and inflammation in certain diseases.[1] Periostin exerts its function through its ability to interact with proteins in the extracellular matrix,[2] promote fibrillogenesis,[3,4] and elicit signaling through integrin-binding on cell surfaces.[5,6] Periostin also plays a role in the pathogenesis of the inflammatory diseases atopic dermatitis, asthma, and psoriasis. In atopic dermatitis, dermal fibroblasts overexpress periostin in response to the Th2 cytokines IL-4 and IL-13 that are essential for the atopic dermatitis pathogenesis, and via integrin-binding on keratinocytes in the epidermis periostin elicits a cellular response that maintains the Th2 inflammation.[7] Simple models of atopic disease have been generated by treating keratinocytes or lung fibroblasts *in vitro* with Th2 cytokines.[8−10] In several cancer types, periostin is overexpressed in tumor or stromal tissue and is found to promote metastasis.[11] Studies using monoclonal antibodies against epitopes on the C-terminal domain (CTD) of periostin show inhibition of general and cancer-associated functions of periostin like cell adherence, proliferation, cell migration, tumor growth, and metastasis, indicating that the CTD of periostin participates in these processes.[12,13] These studies stress the importance of understanding the CTD of periostin, as this might be the key to completely understanding the role of periostin in both health and disease.

Periostin comprises six domains, including an N-terminal cysteine-rich domain of periostin and TGFBIp (CROPT) domain, four fasciclin-1 (FAS-1) domains, and the CTD. X-ray crystallography has been used to obtain the structure of periostin without its CTD.[14] It is commonly accepted that the CTD of periostin is unstructured, but this has never been experimentally validated. The CTD is encoded by exons 15−23, and alternative splicing of exons 17, 18, 19, and 21 produces ten different known isoforms of periostin.[15−17] Distinct expression patterns of periostin splice isoforms have been observed in healthy tissues and cancer, indicating functional differences between the isoforms.[9,18−20] The CTD contains between 93 and 208 residues and makes up 11−26% of the protein, dependent on the splice isoform.

Periostin binds to heparin, and it has been suggested that the C-terminal sequence motif ^{826}SRRRLREGRSQ^{836} encoded by exon 23 is responsible for the interaction.[21] This has not been experimentally verified, and we show that the removal of the sequence motif abolished the heparin-binding capacity,

Received: March 31, 2023
Revised: July 18, 2023
Published: September 13, 2023

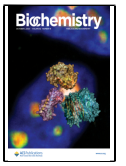

https://doi.org/10.1021/acs.biochem.3c00176
Biochemistry 2023, 62, 2803−2815

confirming its role in heparin binding. Similarly, it is known that periostin interacts with a range of proteins as part of its function.[3,9,22−26] However, the specific domains that facilitate the interactions have only been investigated for a few of its binding partners. To further the understanding of the CTD's function, we explored its interactome in an *in vitro* epidermal atopic dermatitis model by pull-down experiments using full-length and C-terminally truncated periostin as bait. A total of 143 interaction partner candidates were identified that directly or indirectly bound the CTD, among which 140 have not previously been identified. The CTD facilitates both the heparin and protein interactions, and we used biophysical methods to investigate the structure. The results supported the fact that CTD is intrinsically disordered. Despite its lack of structure, the CTD likely participates in the biological function of periostin by binding to other proteins and extracellular matrix components in concert with the four FAS-1 domains.

MATERIALS AND METHODS

Expression and Purification of PN FL and PN ΔCTD. Human periostin was recombinantly expressed in Chinese hamster ovary cells adapted to suspension (CHO-S) as either full-length periostin (PN FL, residue 22−836) or C-terminal truncated periostin (PN ΔCTD, residue 22−628). Both PN FL and PN ΔCTD were expressed with an N-terminal Twin-Strep-tag followed by a TEV cleavage site (39 residues) and were inserted into a pcDNA3.1(+) mammalian expression vector using NheI and AflII restriction sites. The signal peptide from transforming growth factor-beta-induced protein (TGFBIp) was used to improve expression levels. CHO-S cells were maintained in suspension in expression medium (FreeStyle CHO Expression Medium supplemented with 8 mM glutamine, 50 U penicillin, and 50 μg streptomycin) at 37 ° C, 5% CO_2. CHO-S cells were adjusted 4 h prior to transfection to 1×10^6 cells/mL. Cells were transfected using polyethyleneimine (PEI) and DNA in a 4:1 ratio with 1 mg DNA/L cell culture. PEI transfection mix was prepared in 20 mL/L cell culture using an expression medium without antibiotics in the transfection mix. Transfected cells were cultured for five days before the conditioned medium was harvested. The conditioned medium was supplemented with BioLock (IBA Lifesciences), filtered, and applied onto a 5 mL Strep-TactinXT 4Flow column (IBA Lifesciences). The column was washed with buffer A1 (150 mM NaCl, 100 mM Tris−HCl, 1 mM EDTA, pH 8.0) and protein was eluted with Buffer BXT (IBA Lifesciences).

Expression and Purification of PN CTD, PN FAS-CTD, and PN FAS-CTD ΔArg. The CTD of periostin was recombinantly expressed in *E. coli* as CTD alone, with the preceding FAS1-4 domain (PN FAS-CTD, residue 496−836), and PN FAS-CTD with a deletion of the nine penultimate RRRLREGRS residues (PN FAS-CTD ΔArg). All three constructs contain an N-terminal Twin-Strep-tag followed by a TEV cleavage site and were inserted into pET-22b(+) using NcoI and XhoI restriction sites in frame with the PelB signal peptide. One Shot BL21(DE3) Chemically Competent *E. coli* (Thermo Fisher Scientific) were transformed following manufacturer's protocol, and a single colony was picked for overnight culture before inoculating with Terrific Broth for expression. Expression was induced with 0.5 mM isopropyl β-D-1-thiogalactopyranoside (IPTG) at an OD_{600} of 1.0. Cells were pelleted after expression for 3.5 h at 37 °C, 250 rpm, by centrifugation at 3400 × g for 10 min and stored at −70 ° C. The bacteria pellet was thawed and resuspended in 10 mL of buffer A1 supplemented with one complete protease inhibitor cocktail tablet per liter bacteria culture and sonicated using a Q700 sonicator (Qsonica) for 3 × 6 min with 1 s cycles at 16% amplitude while kept on ice. After sonication, the lysate was spun at 25,000 × g at 4 ° C for 20 min and the supernatant was collected, incubated with BioLock (IBA Lifesciences), and filtered before being applied to a StrepTactinXT 4Flow 1 mL column (IBA Lifesciences). The column was washed with 10 column volumes of buffer A1 supplemented with 1 M NaCl before elution with buffer BXT (IBA Lifesciences). To further improve the purity of PN FAS-CTD, this sample was concentrated with Amicon Ultra-15 Centrifugal Filter Unit (10,000 Da MW cut-off) and applied to a Superdex 75 Increase 10/300 GL (Cytiva) gel filtration column equilibrated in buffer A2 (20 mM Tris, 150 mM NaCl, pH 7.4).

Small-Angle X-Ray Scattering (SAXS). SAXS measurements were performed at the laboratory instrument at Aarhus University, Denmark. It is an optimized version of the NanoSTAR instrument from Bruker AXS[27,28] with a gallium metal jet X-ray source from Excillum AB.[29] It has a homebuilt scatter less pinhole[30,31] in front of the sample and an automated sample handler based on a Gilson GX-271 injector, which is connected to a homebuilt flow-through capillary system. The sample and the corresponding buffer for background subtraction were both measured for 3600 s at 20 °C. The background-subtracted intensity was obtained, and it was converted to absolute scale by calibration to the scattering from a pure water sample using the SUPERSAXS package (CLP Oliveira and JS Pedersen, unpublished). The intensity $I(q)$ is a function of q, the modulus of the scattering vector, which is $q = (4\pi \sin(\theta))/\lambda$, where 2θ is the scattering angle between the incident and scattered beam and $\lambda = 1.34$ Å is the wavelength of the K_α Ga radiation. The data were plotted in Guinier and Kratky plots[32] and further processed by performing an indirect Fourier transformation, which gives the pair distance distribution function $p(r)$.[33,34] This function is a histogram of distances between pairs of points within the particles weighted by the excess scattering length density at the points. The data were further analyzed using as the starting point a model predicted by AlphaFold[35] and performing rigid body refinement on the structure using a home-written program,[36−38] which takes a hydration layer into account and uses connectivity and excluded volume restraints. The structure was divided into several bodies, and the program performs random searches with soft restraint for connectivity of the structure, and it also considers excluded volume interactions between the bodies. The predicted structure contains one well-folded domain and extended random-coil parts. In the optimization, the globular domain was used as one of the bodies, and the random-coil part was divided into nine further bodies to allow for flexibility during the optimization. The residues range of the bodies were 1−19, 20−41, 42−192, 193−215, 216−239, 240−260, 261−288, 289−313, 314−357, 358−380. Twenty independent runs were performed, and the structures were aligned for the residues in the globular domain and compared. Before each run, the structure was randomized. It turned out that the data could not be fitted without considering a weak dimerization. Therefore, a structure factor $S(q) = 1 + (N - 1)\sin(qD)/qD$ was used.[39] In the expression, N is the average of the number of proteins in the complex, and D is the distance between the two copies in the dimer. In the

https://doi.org/10.1021/acs.biochem.3c00176
Biochemistry 2023, 62, 2803−2815

calculation of the intensity, the structure factor was included in the decoupling approximation.[40]

$$I(q) = P(q) + \frac{\langle A(q)\rangle^2}{P(q)}[S(q) - 1]$$

where $P(q)$ is the form factor including the hydration layer and $\langle A(q)\rangle$ is the orientationally average scattering amplitude also including the hydration layer where "$\langle \mid \rangle$" symbolizes the averaging. For the calculation of $P(q)$, the Debye equation[41] is used using an average form factor for all non-hydrogen atoms:

$$P(q) = \exp(-q^2\sigma^2) \sum_{i,j} b_i b_j \frac{\sin(qd_{ij})}{qd_{ij}}$$

where σ = 1.0 Å, b_i is, respectively, equal to the average excess scattering length of non-hydrogen atoms for the protein and equal to an average excess scattering length for a hydration dummy atom, and d_{ij} is the distance between the i'th and the j'th atom. The corresponding amplitude is

$$\langle A(q)\rangle = \exp\left(-\frac{q^2\sigma^2}{2}\right) \sum_i b_i \frac{\sin(qd_{i,\mathrm{CM}})}{qd_{i,\mathrm{CM}}}$$

where $d_{i,\mathrm{CM}}$ is the distance of the i'th atom from the scattering center of mass. During the optimization of the structure, the two parameters of the structure factor, N and D, were also optimized.

Circular Dichroism (CD) Spectroscopy. CD experiments were performed using a Chirascan-plus CD spectropolarimeter (Applied Photophysics, Leatherhead, UK). PN FAS-CTD (40 μL, 2.5 mg/mL in TBS) was measured using a 0.1 mm quartz cuvette (Hellma, Switzerland) at ambient temperature (21.5 °C). Three scan repeats were performed in the far-UV range (190−260 nm) with a step size of 0.5 nm, 1 nm bandwidth, and 2 s time per point. The scan repeats were averaged into a single spectrum and deconvoluted with DichroWeb server[42] using the CDSSTR software package[43] with Protein Reference Data Set 7[42,44] to obtain the secondary structure patterns. The CDSSTR program provides multiple solutions for the content fraction of α-helical, β-sheet, turn, and unordered structural elements, where the α-helix and β-sheet are either classified as regular or distorted; however, to simplify the analysis, the regular and distorted elements are combined into single parameters, namely, α-helix and β-sheet. The error was calculated by finding the standard mean deviation between the values for each structural element within the entirety of the 172 possible solutions found for this spectrum. Mapping of distribution of secondary structure elements was performed for the AlphaFold model using STRIDE.[45]

Limited Proteolysis. The proteolytic susceptibility of the recombinant periostin proteins was investigated by limited proteolysis. Samples containing 1 μg of periostin (PN FL, PN ΔCTD, or PN FAS-CTD) were mixed with porcine trypsin (Promega) in molar ratios of 1:800, 1:400, 1:160, 1:80, 1:40, 1:25, 1:8 trypsin−PN in a total volume of 40 μL of buffer A1 and incubated for 15 min at 37 ° C. The proteolytic activity was then terminated by the addition of 2 mM PMSF. Samples were analyzed by reducing sodium dodecyl sulfate-polyacrylamide gel electrophoresis (SDS-PAGE).

N-Terminal Sequencing. Samples of PN FAS-CTD were incubated with trypsin as previously described, separated by reducing SDS-PAGE, and transferred to a polyvinylidene difluoride membrane. Two bands of interest were excised and applied to TFA-treated glass fiber membranes. Automated Edman degradation was performed on a PPSQ-31B protein sequencer (Shimadzu Biotech) with in-line phenylthiohydantoin analysis on an LC-20AT HPLC system. Data were obtained using Shimadzu PPSQ-31B software, and the sequences were determined manually from the UV 269 nm chromatograms.

Heparin Interaction. Heparin affinity chromatography was used to validate the putative heparin-binding site of periostin. A 1 mL HiTrap Heparin HP column (GE Healthcare life sciences) was equilibrated in buffer A (10 mM NaH_2PO_4 pH 7) before 50 μg of PN FL, PN ΔCTD, PN FAS-CTD, or PN FAS-CTD ΔArg were applied. The proteins were eluted with a 30 min linear gradient from 0 to 100% buffer B (10 mM NaH_2PO_4, 1 M NaCl, pH 7). Proteins were monitored at OD_{220} or OD_{280}. In order to elute any residual protein, 2 M NaCl was applied to the column. The collected fractions were analyzed by SDS-PAGE.

Cultivation of NTERT Cells. The immortalized human keratinocyte cell line NTERT1[46] was kindly provided by the laboratory of Ellen H. van den Bogaard (Radboud University Medical Center). The NTERT1 cells were cultured at 37 ° C, 5% CO_2 in serum-free KBM Gold Keratinocyte Growth Basal Medium, calcium, and phenol red-free (Lonza) supplemented with 50 U/mL penicillin, 50 μg/mL streptomycin, and KGM Gold keratinocyte Growth Medium SingleQuots Supplements and Growth factors (Lonza). The cells were supplied with new medium every 2−3 days and subcultured at 70% confluence. To obtain a useful pull-down matrix, NTERT1 cells were seeded at 0.2 × 10^5 cells/cm^2 and cultivated for 17 days in basal medium supplemented with 1.5 mM $CaCl_2$ to allow differentiation of the keratinocytes. The differentiated keratinocytes were cultured for three days in the basal medium supplemented with 10 ng/mL IL-4 and -13 that were harvested and used as the pull-down matrix.

Sample Preparation for LC−MS/MS Label-Free Quantification of the NTERT1 Conditioned Medium. The relative protein abundance present in the conditioned medium from NTERT1 cells treated with IL-4 and -13 vs nontreated NTERT cells was analyzed using LC−MS/MS. First, the conditioned medium was lyophilized, solubilized in denaturation buffer (8 M urea, 100 mM ammonium bicarbonate (Ambic), pH 8), supplemented with 45 mM DTT, and incubated 30 min at RT. Next, to alkylate reduced cysteine residues, 80 mM iodoacetamide was added, and the samples were incubated 30 min at RT. Additional DTT was added to a final concentration of 90 mM to quench iodoacetamide and urea was diluted to 1 M by adding 100 mM Ambic before adding MS-grade trypsin (Promega) in a 1:25 w/w ratio. Samples were digested overnight at 37 ° C and the next day acidified by the addition of formic acid and desalted using Empore Octadecyl C18 reverse phase membranes stage tips as described.[47]

Pull-Down and Sample Preparation for LC−MS/MS. To identify potential interaction partners of periostin CTD, the recombinant PN FL, PN ΔCTD, and PN CTD were used as bait, and the conditioned medium from differentiated NTERT1 cells treated with IL-4/-13 was used as pull-down matrix. MagStrep "type 3" XT 5% bead suspension (IBA Lifesciences) was coupled with 0.85 nmol of PN FL, PN ΔCTD, or PN CTD following the manufacturer's protocol. Coupled beads were incubated with 500 μL pull-down matrix for 60 min at RT rotating and were washed in 3 × 200 μL

https://doi.org/10.1021/acs.biochem.3c00176
Biochemistry 2023, 62, 2803−2815

buffer A1 before interaction partners were eluted in 2 × 25 μL Buffer BXT (IBA Lifesciences). The pull-down was performed in triplicates.

Tryptic digests of eluates for LC−MS/MS analysis were performed on spin filters to remove biotin. Eluates were lyophilized and resuspended in denaturation buffer followed by reduction in 50 mM DTT for 30 min and alkylation in 100 mM iodoacetamide for 30 min. Proteins were captured on Vivacon 500 ultrafiltration spin filter columns (10,000 MW cut-off) and washed twice with 100 μL of denaturation buffer. Urea was removed with 50 mM Ambic pH 8 before 500 ng of MS-grade trypsin (Promega) in 100 μL of 50 mM Ambic pH 8 was added. The samples were vortexed and incubated overnight at 37 ° C. Peptides were collected in a new collection tube by centrifugation at 14,000 × *g* for 30 min before the addition of 50 μL of 500 mM NaCl to the filter and additional centrifugation for 10 min. Samples were desalted using Empore Octadecyl C18 reverse phase membranes stage tips as described.[47]

Label-Free Quantification Using LC−MS/MS. Samples from the conditioned medium and the pull-down experiment were analyzed on an Orbitrap Eclipse Tribrid Mass Spectrometer (Thermo Fisher Scientific) coupled to an Easy-nLC 1200 (Thermo Fisher Scientific) with a 5 cm trap column and a 15 cm analytical column packed in-house with ReproSil-Pur 120 C18-AQ 3 μm (Dr. Maisch GmbH). The flow rate was 250 nL/min, and peptides were eluted with a 50 min or a 20 min gradient from 6 to 44% solvent B (80 acetonitrile, 0.1% formic acid) for the conditioned medium or pull-down samples, respectively. Each replicate was analyzed twice to obtain technical duplicates.

The spectra obtained from LC−MS/MS analysis were analyzed with Proteome Discoverer (version 2.5, Thermo Fisher Scientific). Spectra were searched using the SequestHT search engine against the SwissProt *Homo sapiens* protein sequence database (SwissProt TaxID = 9606) (v2017-10-25) with search parameters; trypsin as protease; up to two missed cleavages; carbamidomethylation of cysteine set as a static modification; methionine oxidation, N-terminal acetylation, and methionine loss set as dynamic modifications; precursor mass tolerance at 10 ppm; fragment mass tolerance at 0.2 Da; FDR of 1%. In order to identify proteins that changed in abundance by treatment with IL-4 and IL-13, we used the search results to perform label-free quantification with the following parameters: unique peptides only; precursor abundance based on intensity; no scaling; normalization to total peptide amount using all peptides; protein ratio calculation based on protein abundance; low abundance resampling imputation of missing values; and ANOVA statistical analysis. Only proteins with ≥2 unique peptides and ≥4 peptide spectra match. Criteria for the difference in abundance were 2-fold relative abundance in treated vs nontreated samples with *p*-value <0.05. To identify interaction partners from the pull-down experiment, search results were used to perform label-free quantification with parameters; unique peptides only; precursor abundance based on intensity; no scaling; no normalization; protein ratio calculation based on protein abundance; low abundance resampling imputation of missing values; and ANOVA statistical analysis. Only proteins with ≥2 unique peptides, ≥4 peptide spectrum matches, and identification/feature detection in ≥60% of the replicates were considered in the analysis. Criteria for CTD interaction partners were >5-fold relative abundance in PN FL vs PN ΔCTD and PN CTD vs PN ΔCTD samples with adjusted *p*-value <0.05. Enrichment analysis of interaction partners was performed using GOrilla[48] with an adjusted *p*-value <0.05 as the threshold for enrichment. A list of all identified proteins in NTERT1 conditioned medium from a separate LC−MS/MS analysis was used as a background in the enrichment analysis.

Native PAGE Interaction Assay. Native PAGE of NTERT conditioned medium incubated with PN CTD and PN FAS-CTD was performed to complement the pull-down experiment. Conditioned medium (25 μL) from differentiated NTERT1 cells treated with IL-4/-13 was mixed with 5 μg of PN CTD or PN FAS-CTD in a volume of 35 μL and incubated for 60 min at RT. Samples were analyzed by native PAGE together with PN CTD alone (5 μg), FAS-CTD alone (5 μg), and conditioned medium alone (25 μL). The native PAGE was stained with Coomassie Brilliant Blue for subsequent in-gel digestion and LC−MS/MS analysis of gel bands.

For the in gel-digestion, gel bands were excised and incubated for 15 min at RT with 20 mM DTT. The buffer was removed, and gel pieces were incubated for 15 min at RT with 40 mM iodoacetamide followed by 15 min in 50% acetonitrile and 15 min in 100% acetonitrile to dehydrate the gel pieces. They were rehydrated in 100 mM Ambic before dehydration using 100% acetonitrile and dried in a speedvac. A total of 0.25 μg MS grade trypsin (Promega) in 100 μL of Ambic was added to the dry gel pieces before they were incubated overnight at 37 ° C. The peptides were desalted using Empore Octadecyl C18 reverse phase membranes stage tips as described[47] and analyzed on an Orbitrap Eclipse Tribrid mass spectrometer (Thermo Fisher Scientific) with a 20 min gradient as described above. MS data were analyzed with Proteome Discoverer. Spectra were searched using the SequestHT search engine against the SwissProt *Homo sapiens* protein sequence database (SwissProt TaxID = 9606) (v2017-10-25) with the recombinant PN CTD sequence added with search parameters; trypsin as protease; up to two missed cleavages; carbamidomethylation of cysteine set as a static modification; methionine oxidation, N-terminal acetylation, and methionine loss set as dynamic modifications; precursor mass tolerance at 10 ppm; fragment mass tolerance at 0.2 Da; and FDR of 1%. Identified proteins were filtered with criteria ≥2 unique peptides and among the 143 potential interaction partners identified in the pull-down experiment. Keratins were excluded due to the risk of being introduced to samples via contamination during sample preparation. Validation of interaction was based on the mobility shift of a potential partner between the lane with the conditioned medium alone and the lanes with PN CTD or PN FAS-CTD in combination with the identification of PN CTD or PN FAS-CTD in the gel band.

RESULTS

Periostin CTD Lacks Tertiary Structure and Contains Only Sparse Secondary Structure Elements. The CTD of periostin (POSTN, UniProtKB Q15063) is predicted by AlphaFold[35] to be disordered. We performed SAXS, CD, and limited proteolysis to investigate this experimentally on PN FAS-CTD (domain structure shown in Figure S1). The CTD was expressed with an N-terminal extension consisting of the fourth FAS-1 domain to increase the solubility of the protein, as the CTD tended to aggregate when expressed alone.

https://doi.org/10.1021/acs.biochem.3c00176
Biochemistry 2023, 62, 2803−2815

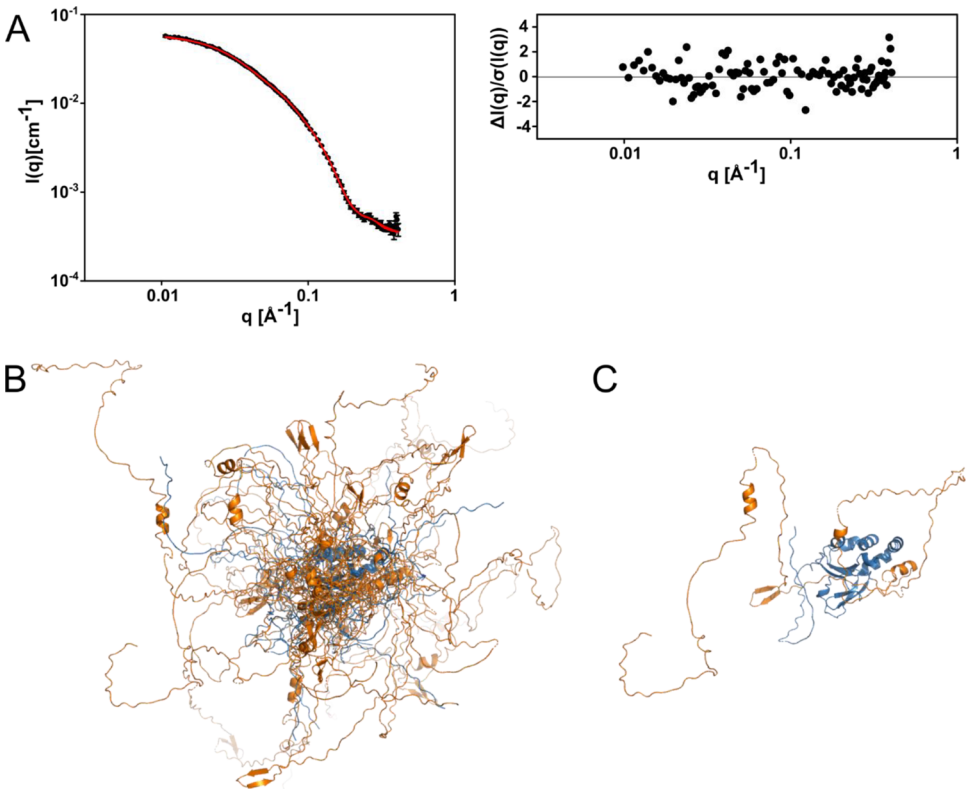

Figure 1. SAXS analysis of PN FAS-CTD revealed that the CTD is disordered. (A) Normalized and background-subtracted SAXS data with a fit for one model shown in red (left) and the corresponding residual plot (right). (B, C) Overlay of all 17 SAXS models aligned by their FAS1−4 domain (B) and the model with the best fit (C) are shown. The FAS1−4 domain is colored blue, and the CTD is colored orange. The N-terminal tag is seen as the disordered blue stretch. The CTD of periostin is disordered and can orient in any direction relative to the FAS1−4 domain.

The normalized background-subtracted data from SAXS are shown in a double logarithmic representation and display a monotonic decrease for increasing q and the characteristics of a Guinier behavior at low values of the scattering vector modulus q with a leveling off of the intensity as q approaches zero[32] (Figure 1A). The Guinier behavior is further confirmed by the linear behavior in the plot of $\ln(I(q))$ versus q^2, where the fit of the straight line gives a radius of gyration of R_g = 45.0 ± 0.5 Å and a forward scattering of $I(0)$ = 0.0600 ± 0.0004 cm^{-1} (Figure S2). A Kratky plot of $qI(q)$ versus q showed that the structure of the protein is globular (the broad peak at low q) with some flexible parts (the relatively high level at high q) (Figure S3). An indirect Fourier transformation gave the fit to the data as shown in Figure S4. The corresponding $p(r)$ function has a maximum of around 30 Å and goes to zero at 160 Å, showing that the particles have a maximum distance within the particles of about 160 Å. The shape of the function resembles the one observed for random coil polymers[49,50] in agreement with the expected flexibility of a large part of the molecule. The indirect Fourier transformation gives additionally that R_g = 47.2 ± 0.3 Å and $I(0)$ = 0.0597 ± 0.0003 cm^{-1}, which agree well with the values from the Guinier analysis. The R_g values are in between that of a fully unfolded protein, 67.9 Å,[51] and a globular protein, 24.5 Å,[52] of the molecular mass as periostin, suggesting a high content of random coil structure. The $I(0)$ value gives a molecular mass of 36 kDa using the expression $M = I(0)N_A/(c\Delta\rho_m^2)$, where N_A is Avogadro's number, c is the concentration in g/mL, and $\Delta\rho_m$ = 2.00 × 10^{10} cm/g is a representative contrast value for proteins. The value is 15% lower than the mass of the monomer (42.5 kDa), probably due to uncertainty in the concentration determination. The normalized Kratky plot of $(qR_g)^2I(q)/I(0)$ versus qR_g is in agreement with the protein having both a globular part (broad maximum at low qR_g) and a flexible part (plateau at larger qR_g) (Figure S3). A summary of the SAXS processing, analysis, and results is displayed in Table S1.

The SAXS data were analyzed further using the AlphaFold prediction of the high-resolution structure as a starting point. The N-terminal tag is unstructured for residues 1−41 and the CTD is unstructured for residues 196−356 except two small regions with a α-helix structure and one small region with the β-sheet structure. The FAS1−4 domain consists of two β-sheets connected by a short α-helix on one side of the domain and six α-helices that make up the other side of the domain. The CTD extends from a β-strand in the center of the FAS1−4 domain. To allow for flexibility, the unstructured N-terminal was divided into two bodies and the CTD into seven bodies, whereas the remaining globular FAS1−4 domain was taken as one body. Rigid-body optimization of the structure with excluded volume and connectivity restraints gave fits to the SAXS data with reduced chi-squared values in the range 1.0−7.6 with most values below 2.0, thus displaying good agreement with the data. Three structures with fits with chi-squared values above 3 were discarded. The reason for the higher chi-squared values for some runs is that the fits are caught in a local minimum, which they cannot escape. One of the fits with a good agreement and the corresponding residue plot is shown (Figure 2C). The overlaid structures are shown after the alignment of the FAS1−4 domain, and the model with the best fit is displayed separately (Figure 1B, C). The different structures show significant variation in the N-terminal and CTD, owing to the lack of tertiary structure and high

https://doi.org/10.1021/acs.biochem.3c00176
Biochemistry 2023, 62, 2803−2815

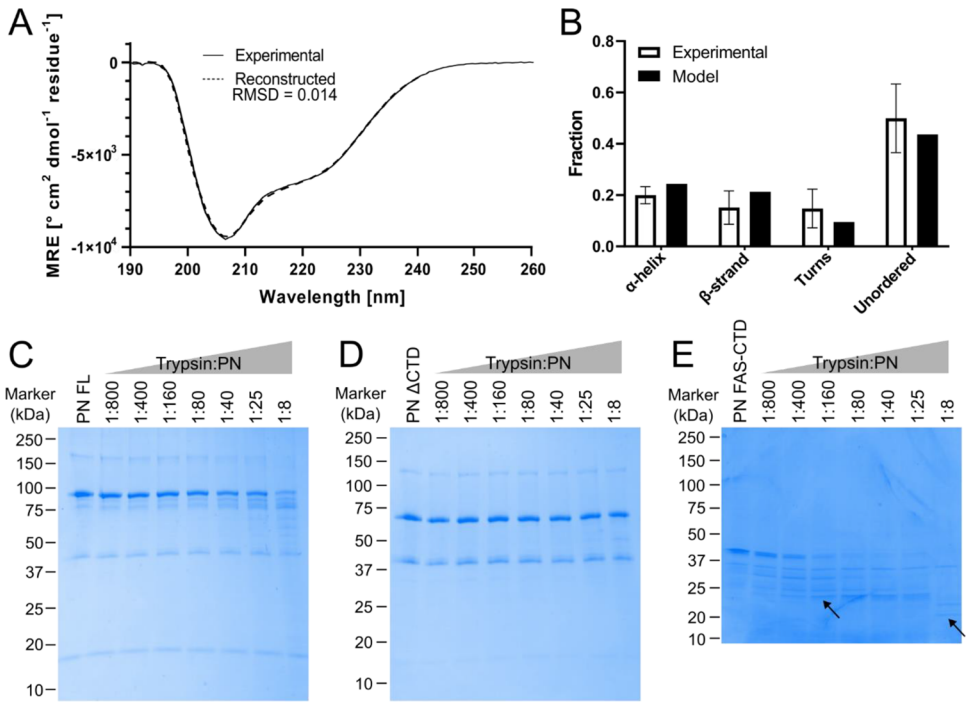

Figure 2. CD spectroscopy and limited proteolysis support the SAXS model of a disordered CTD. (A) CD spectrum of PN FAS-CTD showing the mean of three scans and a reconstructed spectrum used for deconvolution. (B) Fraction of secondary structure elements obtained from deconvolution of the CD spectrum and from the corresponding sequence of the AlphaFold model. Fractions are shown as mean with standard mean deviation. The fraction of secondary structure elements correlates well between the CD data and the model. (C–E) Limited proteolysis of PN FL (C), PN ΔCTD (D), and PN FAS-CTD (E). Each protein is analyzed without trypsin (leftmost lane) and with an increasing molar ratio of trypsin, as indicated above the gel. PN FL (95 kDa) and PN FAS-CTD (43 kDa) are susceptible to trypsin cleavage, while PN ΔCTD (71 kDa) withstands cleavage. Edman degradation of fragments of PN FAS-CTD originating from trypsin cleavage at 1:160 and 1:8 ratio (arrows) showed an intact N-terminal. The CTD is susceptible to protease cleavage, as expected for a disordered region.

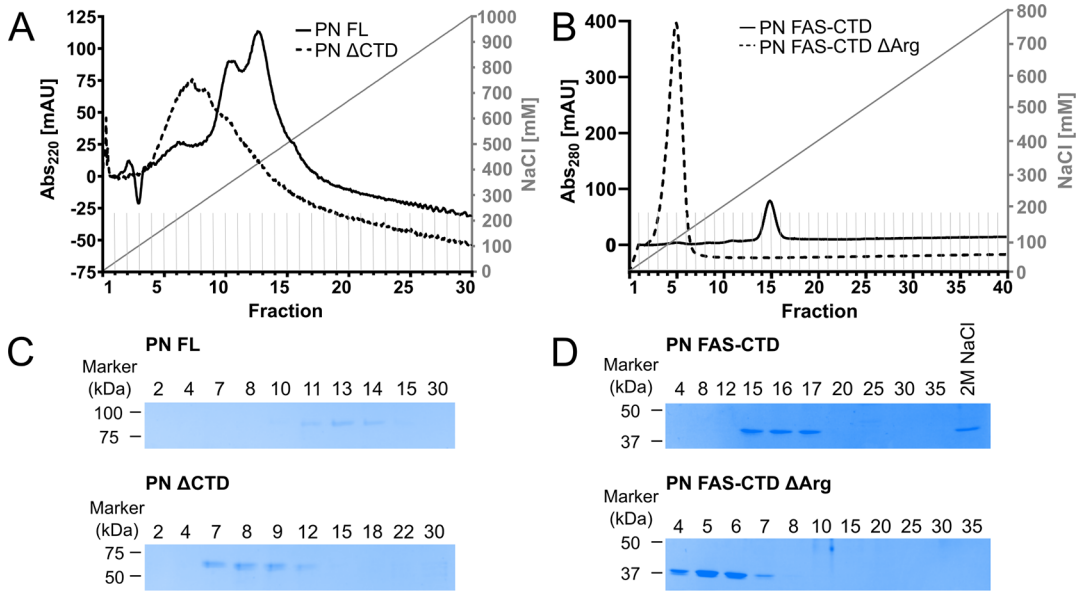

Figure 3. Arginine-rich motif in the C-terminal of periostin is the heparin-binding motif of periostin. (A, B) Heparin affinity chromatography of PN FL and PN ΔCTD (A) and PN FAS-CTD and PN FAS-CTD ΔArg lacking the arginine-rich motif (B). Bound protein was eluted with a linear gradient of NaCl, and fractions were collected as indicated. PN ΔCTD and PN FAS-CTD ΔArg elute earlier than PN FL and PN FAS-CTD, respectively. (C, D) Eluted proteins were analyzed by SDS-PAGE. (C) PN ΔCTD (71 kDa) elutes in fractions 7–9, and PN FL (95 kDa) elutes in fractions 13–14. (D) PN FAS-CTD ΔArg (41 kDa) elutes in fraction 4–7, and PN FAS-CTD (43 kDa) elutes partially in fraction 15–17 and when increasing [NaCl] to 2 M at the end of the gradient. No protein was observed in the 2 M NaCl elution step for the other proteins (not shown). The arginine rich-motif in the C-terminal of periostin binds strongly to heparin and is the main contributor to periostin's heparin affinity.

flexibility. There is likely an even larger variation in the structures present in the ensemble of the sample. However, since the scattering of the individual models agreed well with the data, each of them is a reasonable representation of the

https://doi.org/10.1021/acs.biochem.3c00176
Biochemistry 2023, 62, 2803–2815

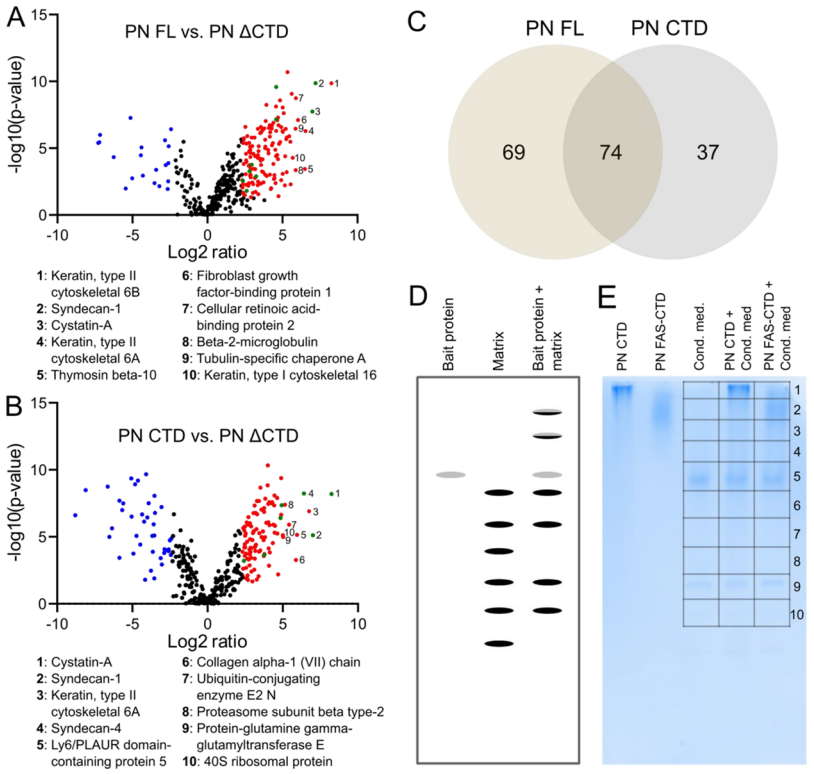

Figure 4. Pull-down and label-free quantification using LC−MS/MS identified 143 potential interaction partners of periostin CTD in a conditioned medium from an *in vitro* epidermal model of atopic dermatitis. (A, B) All of the proteins identified in the pull-down assays are represented in the volcano plots of PN FL vs PN ΔCTD (A) and PN CTD vs ΔCTD (B). Criteria for interaction partners in the LC−MS/MS analysis are ≥2 unique peptides, ≥4 peptide spectrum matches, and >5-fold enriched relative to PN ΔCTD with an adjusted *p*-value <0.05. Under these criteria, proteins that interact with PN FL (n = 143, A) or PN CTD (n = 111, B) are colored red, and proteins that interact with PN ΔCTD (n = 20, A, or n = 42, B) are colored blue. The ten most enriched proteins are numbered and listed below the respective volcano plots. Proteins that are known to be implicated in atopic dermatitis or psoriasis are colored green. (C) Representation of interaction partners from pull-down with PN FL and PN CTD in a Venn diagram. Periostin CTD interacts with a total number of 180 proteins in the matrix, of which 74 interact with both PN FL and PN CTD, 69 interact with PN FL only, and 37 interact with PN CTD only. (D) Schematic of the principle of the native PAGE interaction assay. Interaction partners are identified based on a mobility shift and co-migration with the bait protein. (F) Native PAGE interaction assay using PN CTD and PN FAS-CTD as bait. Bait proteins and conditioned medium were run separately and after being mixed and incubated as specified above the gel. The lanes containing conditioned medium alone, conditioned medium mixed with PN CTD, or PN FAS-CTD were cut into 10 pieces each as illustrated. LC−MS/MS analysis found 22 proteins that made a mobility shift after incubation with PN CTD or PN FAS-CTD and were also identified as interaction partners in the pull-down experiment.

average structure of the ensemble. Thus, we considered that an entire ensemble optimization[53] would not give further insight into the structure. A summary of the SAXS results for the modeling is displayed in Table S2.

CD analysis of PN FAS-CTD supports the conclusions from SAXS. The CD spectrum and the deconvolution into fractions of α-helix, β-strand, turns, and disorder display a high proportion of disorder in PN FAS-CTD (Figure 2A,B). The distribution of α-helix, β-strand, turns, and disorder in the FAS1−4 domain and CTD of the AlphaFold model used for SAXS modeling show good agreement with the experimental CD data, thereby supporting the fact that CTD of periostin is disordered (Figure 2B).

Limited proteolysis of PN FL, PN ΔCTD, and PN FAS-CTD also supports the conclusions from SAXS and CD. Partial proteolytic degradation was observed for PN FL and PN FAS-CTD, while PN ΔCTD was resistant to proteolysis (Figure 2C−E). N-terminal sequencing of PN FAS-CTD fragments at 1:160 and 1:8 ratios (arrows in Figure 2E) showed that the N-terminal is intact, confirming that the cleavage only occurred in the CTD. Combining the results from SAXS, CD, and limited proteolysis, we conclude that the CTD of periostin is intrinsically disordered.

Periostin's Heparin-Binding Affinity Depends on an Arginine-Rich Motif in Its CTD. The heparin-binding motif of periostin is investigated with heparin affinity chromatography of deletion mutants lacking the entire CTD or the C-terminally located arginine-rich motif by monitoring the ionic strength needed for dissociation. A total of 50 μg of PN FL, PN ΔCTD, PN FAS-CTD, or PN FAS-CTD ΔArg (Figure S1) were subjected to heparin affinity chromatography to map the heparin-binding motif of periostin (Figure 3). The heparin-binding assay showed that PN FL bound stronger to heparin than PN ΔCTD as they elute at approximately 400 and 250 mM NaCl, respectively (Figure 3A,C). Deleting the putative heparin-binding motif in the CTD (PN FAS-CTD ΔArg) reduced the heparin-binding affinity significantly compared to PN FAS-CTD (Figure 3B,D). PN FAS-CTD ΔArg interacted weakly with heparin and eluted around 150 mM NaCl. PN FAS-CTD eluted at 350 mM NaCl and at 2 M NaCl at the end of the gradient (not included in the chromatogram). For the other PN proteins, all periostin was eluted during the gradient. These results show that periostin can interact with heparin to

https://doi.org/10.1021/acs.biochem.3c00176
Biochemistry 2023, 62, 2803−2815

some extent without its CTD and that the presence of the CTD increases the binding strength. PN FAS-CTD bound strongly to heparin, while deletion of the arginine-rich motif decreases affinity considerably, supporting that the arginine-rich motif is the heparin-binding motif of periostin.

Total of 143 Interaction Candidates of Periostin's CTD Were Identified in an Atopic Dermatitis Model. The experimental setup of the pull-down study allowed us to identify potential interaction partners of the CTD of periostin. Purified recombinant PN FL, PN ΔCTD, and PN CTD were used as bait coupled to beads via their Twin-Strep-tag. The conditioned medium from an *in vitro* epidermal model of atopic dermatitis was used as a pull-down matrix. This pull-down matrix was chosen based on a mass spectrometry-based label-free quantification analysis comparing the proteins in a conditioned medium from untreated keratinocytes vs keratinocytes treated with the Th2 cytokines IL-4 and IL-13. NTERT1 cells treated with Th2 cytokines have been used as a model of atopic dermatitis by others.[10] The analysis of the conditioned medium found 11 proteins to be upregulated and 27 proteins to be downregulated in the model of atopic dermatitis (Table S3). A total of 1101 proteins were identified in the conditioned medium. In the pull-down experiments comparing the bait proteins PN FL and PN ΔCTD, 143 proteins were found to interact with periostin in a CTD-dependent manner as these were pulled down by PN FL and not PN ΔCTD (Figure 4A). Of the 143 candidates, 54 were exclusively identified in the samples with FL PN as bait, and the additional 89 were >5-fold enriched compared to pull-down with PN ΔCTD. The experiment also identified 20 proteins to interact with periostin in the absence of the CTD as they were pulled down by PN ΔCTD and not PN FL (Figure 4A). In the parallel pull-down experiment comparing the bait proteins PN CTD and PN ΔCTD, 111 proteins interacted with PN CTD and not PN ΔCTD (Figure 4B). Of these 111 candidates, 52 were exclusively identified in the samples with PN CTD as bait, and the additional 59 were >5-fold enriched compared to pull-down with PN ΔCTD. In this experiment, 42 proteins interacted with PN ΔCTD and not PN CTD (Figure 4B). The identified potential interaction partners from PN FL vs PN ΔCTD and from PN CTD vs PN ΔCTD are listed in Tables S4−S7. The two complementary pull-down experiments combined found 180 potential interaction partners of periostin CTD, of which 74 are found to interact with both PN FL and PN CTD (Figure 4C). The proteins in each of the three categories in the Venn diagram (Figure 4C) are listed in Table S8. From these experiments, we put forward a list of 143 proteins that interact with periostin in a CTD-dependent manner, of which 74 can interact with the CTD of periostin alone. Three of the candidates are known interaction partners of periostin, while 140 are novel potential interaction partners of periostin CTD.

A native PAGE experiment with the NTERT1-conditioned medium incubated with PN CTD and PN FAS-CTD was used to confirm a subset of the potential interaction partners identified from the pull-down experiment. In a native PAGE, noncovalent interactions with a certain strength between interacting proteins are preserved during electrophoresis.[54] The noncovalent interactions between PN CTD or PN FAS-CTD and its partners are expected to alter the electrophoretic mobility of both proteins. Identification of proteins using LC−MS/MS throughout the lanes of the conditioned medium alone and conditioned medium incubated with PN CTD or PN FAS-CTD was used to monitor shifts in electrophoretic mobility as illustrated in Figure 4D. The majority of PN CTD migrates as a sharp band in the top of the gel and is unaltered after incubation with the conditioned medium (Figure 4E) while PN FAS-CTD does not migrate as a sharp band, and a slight shift upward is observed after incubation with the conditioned medium (Figure 4E). For both PN CTD and PN FAS-CTD, peptides from these proteins were observed in gel bands 1−9 in the LC−MS/MS analysis showing that it co-migrates with proteins in the conditioned medium. The LC−MS/MS analysis of gel bands led to the identification of 22 proteins that made a mobility shift when incubated with PN CTD or PN FAS-CTD and were also found in the pull-down assay to interact with the CTD of periostin. These are listed in Table S9. In our work, we present 143 potential interaction partners of periostin CTD from a pull-down experiment, among which 22 are validated by this approach.

Enrichment analysis of the proteins interacting with the CTD of periostin show enrichment of proteins with the GO terms "extracellular space" (n = 48), "proteasome core complex" (n = 10), "cytokine-mediated signaling pathway" (n = 26), and "proteasomal ubiquitin-independent protein catabolic process" (n = 10). Enrichment is borderline significant for proteins with the GO terms "regulation of immune system process" (n = 39, adjusted p-value 0.075) and "activation of innate immune response" (n = 16, adjusted p-value 0.076). The proteins from the enriched categories are listed in Table S10. Manual inspection of the list of interaction partners led to the identification of nine proteins that are connected to atopic dermatitis or psoriasis (Table 1), in which periostin is known to be involved in the pathogenesis. The interaction with two of those, protein S100-A9 and heat shock protein HSP 90-alpha, was confirmed in the native PAGE experiment. Additionally, the two proteins quinone oxidoreductase PIG3 and gamma-glutamyl hydrolase were identified as potential binding partners of periostin CTD in the pull-down experiment and were also found to be upregulated in the conditioned medium after treatment of keratinocytes with IL-4 and IL-13 (Tables S3 and S4). Overall, the pull-down experiment provided a list of novel potential interaction partners of periostin CTD, among which some are involved in inflammatory skin diseases.

A manual search of all the identified interaction partners revealed six to be implicated in both atopic dermatitis and psoriasis and three in atopic dermatitis as indicated.

DISCUSSION

The CTD of periostin contains several interesting features, including (i) it has no tertiary structure, (ii) it is alternatively spliced, yielding ten variants, (iii) it contains a heparin-binding motif, and (iv) it is distinct from the short CTD of the paralogue protein TGFBIp that has an otherwise identical domain structure. These features suggest that the CTD of periostin is important for the function of the protein. Here, we provide the first in-depth characterization of the structure and interactome of the periostin CTD.

The structural analysis using SAXS, CD, and limited proteolysis revealed that the CTD of periostin was disordered. In AlphaFold, the CTD of periostin has very low model confidence of predicted local distance difference test (pLDDT < 50), which is often seen for disordered regions. The SAXS analysis yielded 17 models of PN FAS-CTD that all predicted a folded FAS1−4 domain and a disordered CTD (Figure 1B, C).

https://doi.org/10.1021/acs.biochem.3c00176
Biochemistry 2023, 62, 2803−2815

Table 1. Nine Novel CTD Interaction Partners Are Involved in Atopic Dermatitis and Psoriasis

gene name	protein name	atopic dermatitis	psoriasis	pulled down by	reference
S100A7	protein S100-A7	X	X	PN FL	Broome et al.[64]
				PN CTD	Gläser et al.[65]
S100A8	protein S100-A8	X	X	PN FL	Broome et al.[64]
				PN CTD	Wood et al.[66]
					Jin et al.[67]
S100A9	protein S100-A9	X	X	PN FL	Broome et al.[64]
				PN CTD	Jin et al.[67]
SDC1	syndecan-1	X	X	PN FL	Tomas et al.[68]
				PN CTD	
SDC4	syndecan-4	X		PN FL	Nakao et al.[69]
				PN CTD	
CSTA	cystatin-A	X		PN FL	Seguchi et al.[70]
				PN CTD	
HMOX1	heme oxygenase 1	X		PN FL	Kirino et al.[71]
HSP90AA1	heat shock protein HSP 90-alpha	X	X	PN FL	Sitko et al.[72]
					Bregnhøj et al.[73]
LCN2	neutrophil gelatinase-associated lipocalin	X	X	PN FL	Aizawa et al.[74]
				PN CTD	

Periostin and TGFBIp have identical domain compositions and similar overall shapes. The CTD of TGFBIp could not be mapped in the crystal structure of TGFBIp[55] and is also predicted with very low confidence by AlphaFold.[35] The CTD is the most distinct domain between periostin and TGFBIp, although it seems to be disordered in both proteins. Completely disordered proteins or proteins containing disordered regions are common, and their key functionality is usually to engage in protein−protein interactions as they often have a large interactome.[56] The function of the CTD and how the lack of tertiary structure supports its function are still not understood. In this study, a comprehensive interactome of the CTD was identified in line with our classification of it as a disordered region. The variants of the CTD originating from alternative splicing are expected to be disordered as well and to have individual interactomes. We suggest that the lack of structure is a prerequisite for functional variations between the periostin splice isoforms based on the modular nature of the alternatively spliced exons that encode the major part of the CTD. This modularity is difficult to incorporate into a structured domain without disturbing the structure, in which case the splice variants would likely be misfolded and nonfunctional. Thus, we propose the CTD to be a disordered part of periostin that is functionally modified by alternative splicing. Alternative splicing of periostin CTD is a conserved feature found across tetrapod to teleost species,[57] supporting this hypothesis and underlining that this is likely to be important for periostin's function.

The heparin affinity of periostin has previously been suggested based on the presence of a cluster of positively charged basic amino acid residues.[21] In this study, we provide experimental evidence that the C-terminal arginine-rich motif is responsible for periostin's heparin affinity (Figure 3). This arginine-rich motif is hypothesized to interact with negatively charged glycosaminoglycans like heparin sulfate and chondroitin sulfate in the extracellular matrix *in vivo*. Based on the C-terminal location of the heparin-binding motif and the presented proteolytic vulnerability of the CTD (Figure 2C, E), the interaction between periostin and proteoglycans or glycosaminoglycans in the extracellular matrix might be regulated by proteolytic events. Proteolytic processing of periostin CTD has been observed *in vivo* in, e.g., mouse periosteum.[2]

Periostin is known to interact with 16 proteins; itself,[9] fibronectin,[9] tenascin-C,[9] collagen V,[9] TGFBIp,[22] $\alpha_v\beta_3$ and $\alpha_v\beta_5$ integrin,[5,7,58] integrin-linked protein kinase,[59] C2 and C2-like subunits of the trafficking protein particle (TRAPP) complex,[26] the proteoglycans syndecan-1 and syndecan-4,[60] CCN3,[23] the protease BMP-1,[3] laminin γ2,[24] and Notch1.[25] A direct interaction has been observed for fibronectin, tenascin-C, collagen V,[9] BMP-1,[3] and $\alpha_v\beta_3$ and $\alpha_v\beta_5$ integrin,[5] while the others might interact with periostin indirectly. In comparison, TGFBIp is known to interact with 19 proteins, including fibronectin, laminin, and $\alpha_v\beta_3$ and $\alpha_v\beta_5$ integrin.[61]

In this study, we confirmed syndecan-1, syndecan-4, and laminin γ2 as periostin interaction partners and found that they interact via the CTD of periostin. Fibronectin, collagen V, integrin-linked protein kinase, and BMP-1 were present in the pull-down matrix without their expression level being affected by treatment with IL-4 and IL-13 (Table S3) but not identified in the pull-down experiment for either bait protein. TGFBIp interacted with both FL PN and FL ΔCTD in the pull-down experiment with no significant difference. The other known interaction partners were not present in the pull-down matrix.

By using both PN FL and PN CTD as bait in the pull-down experiment, we provide an additional layer of information regarding the nature of the interaction to periostin for the interaction candidates. Of the 143 candidates found to interact with PN FL, 74 also interact with PN CTD (Figure 4C), which provides the information that they interact with the CTD of periostin independent on the CROPT and FAS1 domains of periostin. In contrast, the 69 candidates interacting exclusively with PN FL do so in a way dependent on both the CTD and the N-terminal part of periostin. The 37 proteins that interact with PN CTD and not PN FL are not regarded as physiologically relevant interaction partners since the CTD of periostin is not expected to be present alone *in vivo*. From the orthogonal native PAGE interaction experiment, 22 of the 143 candidates were also observed to interact with the CTD of periostin. Protein S100-A9 and heat shock protein HSP 90-alpha implicated in atopic dermatitis and psoriasis were among these 22 proteins. In the native PAGE, the electric force and resistance moving through the gel will likely break weak interactions, and proteins with a high pI will not enter the gel; therefore, only a subset of the 143 candidates from the pull-down experiment was expected to be observed as interaction partners in the native PAGE experiment.

In addition to syndecan-1 and syndecan-4, glypican-1 was found to interact with periostin CTD. All of them are heparan sulfate proteoglycans and likely interact with periostin through their heparan sulfate chains and the arginine-rich motif in the

https://doi.org/10.1021/acs.biochem.3c00176
Biochemistry 2023, 62, 2803−2815

periostin CTD. Of the 140 novel interaction partners identified in this study, some likely interact indirectly with the CTD of periostin. A recent study maps the interactome of glypican-1.[62] Ten of the glypican-1 interaction partners were also found to interact with periostin CTD in our study. These are listed in Table S11, and it is likely that some of these do not interact directly with periostin but were pulled down via glypican-1. Among the novel potential interaction partners, ten are subunits of the proteasome complex. These significantly stand out among the CTD interaction partners, as seen from the enrichment analysis. Extracellular localization of the 20S proteasome core complex has been observed in multiple body fluids where they are hypothesized to function as ATP- and ubiquitin-independent proteolytic complexes that degrade especially disordered proteins.[63] The proteasome subunits that interact with periostin CTD are part of the 20S proteasome. The interaction between periostin CTD and the 20S proteasome is in line with the presented structural analysis that reveals the CTD to be disordered, making it a substrate for the 20S proteasome. The enrichment analysis also highlighted 26 candidates involved in the "cytokine-mediated signaling pathway." Certain functions of periostin rely on its ability to act as a scaffolding protein.[2,3] A function of the CTD might be to participate in this scaffolding and facilitate the association of cytokines and their receptor.

Among the novel interaction partners, nine are implicated in atopic dermatitis and/or psoriasis (Table 1). These proteins are protein S100A7,[64,65] -A8,[64,66,67] and -A9,[64,67] syndecan-1,[68] syndecan-4,[69] cystatin-A,[70] heme oxygenase 1,[71] heat shock protein HSP 90-alpha,[72,73] and neutrophil gelatinase-associated lipocalin.[74] Heme oxygenase 1 and heat shock protein HSP 90-alpha were found to interact with PN FL, and not PN CTD. The other seven proteins interacted with both PN FL and PN CTD. Overexpression of protein S100A9 in atopic dermatitis correlates with disease severity, and binding of protein S100A9 to the receptor of advanced glycation end products (RAGE) on keratinocytes induces expression of the Th2-cytokine IL-33 that is one of the drivers of atopic dermatitis.[67,75] RAGE is seen to associate with integrin $\alpha_v\beta_3$,[76] an interaction partner of periostin, thereby leading to the hypothesis that the observed interaction between periostin CTD and protein S100A9 could facilitate protein S100A9-induced IL-33 expression in atopic dermatitis with periostin acting as a scaffold bringing protein S100A9 in contact with its receptor. In psoriasis, protein S100A7 acts in a similar way where binding to RAGE on keratinocytes leads to increased levels of mature IL-1α, a critical cytokine in psoriasis pathogenesis.[77] This supports the theory of periostin acting as a scaffolding protein that facilitates the association of RAGE and its ligands in atopic dermatitis and psoriasis. The finding that several proteins involved in atopic dermatitis and psoriasis interact with periostin CTD gives a new lead to study the role of periostin in these diseases.

CONCLUSIONS

In this study, we present the first experimental structural investigation of the periostin CTD and find it completely disordered across 17 models based on SAXS data. These models of periostin CTD are supported by CD and limited proteolysis experiments. We also provide the first experimental data to map the heparin-binding site of periostin to the arginine-rich motif in the very C-terminal of periostin. This heparin-binding site is likely responsible for the CTD-dependent interactions with the heparin sulfate proteoglycans syndecan-1, syndecan-4, and glypican-1 reported here. We report 143 proteins from an *in vitro* epidermal atopic dermatitis model to be potential interaction partners of periostin CTD. Three of these, syndecan-1, syndecan-4, and laminin γ2, are known interaction partners of periostin, and our study reveals the interaction to be CTD-dependent. Nine of the candidates are involved in atopic dermatitis and psoriasis. These novel disease-implicated interaction partners can provide new perspectives in understanding the role of periostin in these diseases. Based on our study, we suggest that CTD is involved in multiple protein−protein interactions as part of the scaffolding role of periostin. Furthermore, we propose that the disordered nature of periostin CTD is a prerequisite for functional variation between splice variants of periostin.

ASSOCIATED CONTENT

Data Availability Statement

The mass spectrometry raw data and Proteome Discoverer result files have been deposited to the ProteomeXchange Consortium via the PRIDE partner repository with the data set identifier PXD040164 and 10.6019/PXD040164.

Supporting Information

The Supporting Information is available free of charge at https://pubs.acs.org/doi/10.1021/acs.biochem.3c00176.

Schematic of recombinant periostin proteins; Guinier plot; normalized Kratky plot; indirect Fourier transformation of SAXS data; tables with details from SAXS data collection, processing, and analysis; label-free quantification results; enrichment analysis; and periostin CTD/glypican-1 shared interaction partners (PDF)

AUTHOR INFORMATION

Corresponding Author

Jan J. Enghild − *Department of Molecular Biology and Genetics, Aarhus University, Aarhus C 8000, Denmark;* orcid.org/0000-0001-9292-9172; Email: jje@mbg.au.dk

Authors

Christian E. Rusbjerg-Weberskov − *Department of Molecular Biology and Genetics, Aarhus University, Aarhus C 8000, Denmark*

Mette Liere Johansen − *Department of Molecular Biology and Genetics, Aarhus University, Aarhus C 8000, Denmark*

Jan S. Nowak − *Department of Molecular Biology and Genetics and Interdisciplinary Nanoscience Center (iNANO), Aarhus University, Aarhus C 8000, Denmark*

Daniel E. Otzen − *Department of Molecular Biology and Genetics and Interdisciplinary Nanoscience Center (iNANO), Aarhus University, Aarhus C 8000, Denmark;* orcid.org/0000-0002-2918-8989

Jan Skov Pedersen − *Department of Chemistry and Interdisciplinary Nanoscience Center (iNANO), Aarhus University, Aarhus C 8000, Denmark;* orcid.org/0000-0002-7768-0206

Nadia Sukusu Nielsen − *Department of Molecular Biology and Genetics, Aarhus University, Aarhus C 8000, Denmark*

Complete contact information is available at: https://pubs.acs.org/10.1021/acs.biochem.3c00176

Author Contributions

Conceptualization and methodology, C.E.R.W., J.J.E., N.S.N.; investigation and formal analysis, C.E.R.W., M.L.J., J.S.N.,

https://doi.org/10.1021/acs.biochem.3c00176
Biochemistry 2023, 62, 2803−2815

D.E.O., J.S.P., and N.S.N.; writing original draft, C.E.R.W.; writing, review, and editing, D.E.O., J.S.P., J.J.E., and N.S.N.; funding acquisition, J.J.E.

Funding

This work was supported by the LEO Foundation, the VELUX Foundation (00014557), the Novo Nordisk Foundation (BIO-MS) (NNF18OC0032724), and the Independent Research Foundation Denmark (8021-00208B).

Notes

The authors declare no competing financial interest.

■ ACKNOWLEDGMENTS

We thank Ida B. Thøgersen for performing the automated Edman degradations.

■ ABBREVIATIONS

CD, circular dichroism; CROPT, cysteine-rich domain of periostin and TGFBIp; CTD, C-terminal domain; FAS-1, fasciclin-1; LC−MS/MS, liquid chromatography tandem mass spectrometry; PEI, polyethyleneimine; RAGE, receptor of advanced glycation end products; SAXS, small-angle X-ray scattering; TGFBIp, transforming growth factor-beta-induced protein

■ REFERENCES

(1) Conway, S. J.; Izuhara, K.; Kudo, Y.; Litvin, J.; Markwald, R.; Ouyang, G.; Arron, J. R.; Holweg, C. T. J.; Kudo, A. The role of periostin in tissue remodeling across health and disease. *Cell. Mol. Life Sci.* **2014**, *71*, 1279−1288.

(2) Kii, I.; Nishiyama, T.; Li, M.; Matsumoto, K.; Saito, M.; Amizuka, N.; Kudo, A. Incorporation of tenascin-C into the extracellular matrix by periostin underlies an extracellular meshwork architecture. *J. Biol. Chem.* **2010**, *285*, 2028−2039.

(3) Maruhashi, T.; Kii, I.; Saito, M.; Kudo, A. Interaction between periostin and BMP-1 promotes proteolytic activation of lysyl oxidase. *J. Biol. Chem.* **2010**, *285*, 13294−13303.

(4) Norris, R.; Damon, B.; Mironov, V.; Kasyanov, V.; Ramamurthi, A.; Moreno-Rodriguez, R.; Trusk, T.; Potts, J. D.; Goodwin, R. L.; Davis, J.; Hoffman, S.; Wen, X.; Sugi, Y.; Kern, C. B.; Mjaatvedt, C. H.; Turner, D. K.; Oka, T.; Conway, S. J.; Molkentin, J. D.; Forgacs, G.; Markwald, R. R. Periostin regulates collagen fibrillogenesis and the biomechanical properties of connective tissues. *J. Cell. Biochem.* **2007**, *101*, 695−711.

(5) Gillan, L.; Matei, D.; Fishman, D. A.; Gerbin, C. S.; Karlan, B. Y.; Chang, D. D. Periostin secreted by epithelial ovarian carcinoma is a ligand for alpha(V)beta(3) and alpha(V)beta(5) integrins and promotes cell motility. *Cancer Res.* **2002**, *62*, 5358−5364.

(6) Khurana, S.; Schouteden, S.; Manesia, J. K.; Santamaria-Martínez, A.; Huelsken, J.; Lacy-Hulbert, A.; Verfaillie, C. M. Outside-in integrin signalling regulates haematopoietic stem cell function via Periostin-Itgav axis. *Nat. Commun.* **2016**, *7*, 13500.

(7) Masuoka, M.; Shiraishi, H.; Ohta, S.; Suzuki, S.; Arima, K.; Aoki, S.; Toda, S.; Inagaki, N.; Kurihara, Y.; Hayashida, S.; Takeuchi, S.; Koike, K.; Ono, J.; Noshiro, H.; Furue, M.; Conway, S. J.; Narisawa, Y.; Izuhara, K. Periostin promotes chronic allergic inflammation in response to Th2 cytokines. *J. Clin. Investig.* **2012**, *122*, 2590−2600.

(8) Park, A. Y.; Bourtembourg, M.; Chrétien, A.; Hubaux, R.; Lancelot, C.; Salmon, M.; Fitton, J. H. Modulation of Gene Expression in a Sterile Atopic Dermatitis Model and Inhibition of Staphylococcus aureus Adhesion by Fucoidan. *Dermatopathology* **2021**, *8*, 69−83.

(9) Takayama, G.; Arima, K.; Kanaji, T.; Toda, S.; Tanaka, H.; Shoji, S.; McKenzie, A. N.; Nagai, H.; Hotokebuchi, T.; Izuhara, K. Periostin: a novel component of subepithelial fibrosis of bronchial asthma downstream of IL-4 and IL-13 signals. *J. Allergy Clin. Immunol.* **2006**, *118*, 98−104.

(10) Smits, J. P. H.; Niehues, H.; Rikken, G.; van Vlijmen-Willems, I.; van de Zande, G.; Zeeuwen, P.; Schalkwijk, J.; van den Bogaard, E. H. Immortalized N/TERT keratinocytes as an alternative cell source in 3D human epidermal models. *Sci. Rep.* **2017**, *7*, 11838.

(11) Dorafshan, S.; Razmi, M.; Safaei, S.; Gentilin, E.; Madjd, Z.; Ghods, R. Periostin: biology and function in cancer. *Cancer Cell Int.* **2022**, *22*, 315.

(12) Fujikawa, T.; Sanada, F.; Taniyama, Y.; Shibata, K.; Katsuragi, N.; Koibuchi, N.; Akazawa, K.; Kanemoto, Y.; Kuroyanagi, H.; Shimazu, K.; Rakugi, H.; Morishita, R. Periostin Exon-21 Antibody Neutralization of Triple-Negative Breast Cancer Cell-Derived Periostin Regulates Tumor-Associated Macrophage Polarization and Angiogenesis. *Cancers* **2021**, *13*, 5072.

(13) Kyutoku, M.; Taniyama, Y.; Katsuragi, N.; Shimizu, H.; Kunugiza, Y.; Iekushi, K.; Koibuchi, N.; Sanada, F.; Oshita, Y.; Morishita, R. Role of periostin in cancer progression and metastasis: inhibition of breast cancer progression and metastasis by anti-periostin antibody in a murine model. *Int. J. Mol. Med.* **2011**, *28*, 181−186.

(14) Liu, J.; Zhang, J.; Xu, F.; Lin, Z.; Li, Z.; Liu, H. Structural characterizations of human periostin dimerization and cysteinylation. *FEBS Lett.* **2018**, *592*, 1789−1803.

(15) Bai, Y.; Nakamura, M.; Zhou, G.; Li, Y.; Liu, Z.; Ozaki, T.; Mori, I.; Kakudo, K. Novel isoforms of periostin expressed in the human thyroid. *Jpn. Clin. Med.* **2010**, *1*, 13−20.

(16) Morra, L.; Rechsteiner, M.; Casagrande, S.; Duc Luu, V.; Santimaria, R.; Diener, P. A.; Sulser, T.; Kristiansen, G.; Schraml, P.; Moch, H.; Soltermann, A. Relevance of periostin splice variants in renal cell carcinoma. *Am. J. Pathol.* **2011**, *179*, 1513−1521.

(17) Morra, L.; Rechsteiner, M.; Casagrande, S.; von Teichman, A.; Schraml, P.; Moch, H.; Soltermann, A. Characterization of periostin isoform pattern in non-small cell lung cancer. *Lung Cancer* **2012**, *76*, 183−190.

(18) Nance, T.; Smith, K. S.; Anaya, V.; Richardson, R.; Ho, L.; Pala, M.; Mostafavi, S.; Battle, A.; Feghali-Bostwick, C.; Rosen, G.; Montgomery, S. B. Transcriptome analysis reveals differential splicing events in IPF lung tissue. *PLoS One* **2014**, *9*, No. e92111.

(19) Cai, L.; Brophy, R. H.; Tycksen, E. D.; Duan, X.; Nunley, R. M.; Rai, M. F. Distinct expression pattern of periostin splice variants in chondrocytes and ligament progenitor cells. *FASEB J.* **2019**, *33*, 8386−8405.

(20) Nanri, Y.; Nunomura, S.; Watanabe, T.; Ohta, S.; Yamaguchi, Y.; Izuhara, K. Expression profile of periostin isoforms in systemic sclerosis. *J. Dermatol. Sci.* **2021**, *104*, 210−212.

(21) Sugiura, T.; Takamatsu, H.; Kudo, A.; Amann, E. Expression and characterization of murine osteoblast-specific factor 2 (OSF-2) in a baculovirus expression system. *Protein Expression Purif.* **1995**, *6*, 305−311.

(22) Kim, B.-Y.; Olzmann, J. A.; Choi, S.-I.; Ahn, S. Y.; Kim, T.-I.; Cho, H.-S.; Suh, H.; Kim, E. K. Corneal Dystrophy-associated R124H Mutation Disrupts TGFBI Interaction with Periostin and Causes Mislocalization to the Lysosome*. *J. Biol. Chem.* **2009**, *284*, 19580−19591.

(23) Takayama, I.; Tanabe, H.; Nishiyama, T.; Ito, H.; Amizuka, N.; Li, M.; Katsube, K. I.; Kii, I.; Kudo, A. Periostin is required for matricellular localization of CCN3 in periodontal ligament of mice. *J. Cell Commun. Signaling* **2017**, *11*, 5−13.

(24) Nishiyama, T.; Kii, I.; Kashima, T. G.; Kikuchi, Y.; Ohazama, A.; Shimazaki, M.; Fukayama, M.; Kudo, A. Delayed Re-Epithelialization in Periostin-Deficient Mice during Cutaneous Wound Healing. *PLoS One* **2011**, *6*, No. e18410.

(25) Tanabe, H.; Takayama, I.; Nishiyama, T.; Shimazaki, M.; Kii, I.; Li, M.; Amizuka, N.; Katsube, K.-I.; Kudo, A. Periostin Associates with Notch1 Precursor to Maintain Notch1 Expression under a Stress Condition in Mouse Cells. *PLoS One* **2010**, *5*, No. e12234.

(26) Duarte, D. T.; Hul, S.; Sacher, M. A yeast two hybrid screen identifies SPATA4 as a TRAPP interactor. *FEBS Lett.* **2011**, *585*, 2676−2681.

https://doi.org/10.1021/acs.biochem.3c00176
Biochemistry 2023, 62, 2803−2815

(27) Lyngso, J.; Pedersen, J. S. A high-flux automated laboratory small-angle X-ray scattering instrument optimized for solution scattering. *J. Appl. Crystallogr.* **2021**, *54*, 295−305.
(28) Pedersen, J. A flux- and background-optimized version of the NanoSTAR small-angle X-ray scattering camera for solution scattering. *J. Appl. Crystallogr.* **2004**, *37*, 369−380.
(29) Schwamberger, A.; De Roo, B.; Jacob, D.; Dillemans, L.; Bruegemann, L.; Seo, J. W.; Locquet, J. P. Combining SAXS and DLS for simultaneous measurements and time-resolved monitoring of nanoparticle synthesis. *Nucl. Instrum. Methods Phys. Res., Sect. B* **2015**, *343*, 116−122.
(30) Li, Y.; Beck, R.; Huang, T.; Choi, M. C.; Divinagracia, M. Scatterless hybrid metal-single-crystal slit for small-angle X-ray scattering and high-resolution X-ray diffraction. *J. Appl. Crystallogr.* **2008**, *41*, 1134−1139.
(31) Pedersen, J. S. X-ray analyzing system for x-ray scattering analysis. US Patent US9958404B2, European Patent EP13159569.6, 2018.
(32) Jeffries, C. M.; Ilavsky, J.; Martel, A.; Hinrichs, S.; Meyer, A.; Pedersen, J. S.; Sokolova, A. V.; Svergun, D. I. Small-angle X-ray and neutron scattering. *Nat. Rev. Methods Primers* **2021**, *1*, 70.
(33) Glatter, O. A new method for the evaluation of small-angle scattering data. *J. Appl. Crystallogr.* **1977**, *10*, 415−421.
(34) Pedersen, J. S.; Hansen, S.; Bauer, R. The aggregation behavior of zinc-free insulin studied by small-angle neutron scattering. *Eur. Biophys. J.* **1994**, *22*, 379−389.
(35) Varadi, M.; Anyango, S.; Deshpande, M.; Nair, S.; Natassia, C.; Yordanova, G.; Yuan, D.; Stroe, O.; Wood, G.; Laydon, A.; Žídek, A.; Green, T.; Tunyasuvunakool, K.; Petersen, S.; Jumper, J.; Clancy, E.; Green, R.; Vora, A.; Lutfi, M.; Figurnov, M.; Cowie, A.; Hobbs, N.; Kohli, P.; Kleywegt, G.; Birney, E.; Hassabis, D.; Velankar, S. AlphaFold Protein Structure Database: massively expanding the structural coverage of protein-sequence space with high-accuracy models. *Nucleic Acids Res.* **2022**, *50*, D439−D444.
(36) Harwood, S. L.; Lyngsø, J.; Zarantonello, A.; Kjøge, K.; Nielsen, P. K.; Andersen, G. R.; Pedersen, J. S.; Enghild, J. J. Structural Investigations of Human A2M Identify a Hollow Native Conformation That Underlies Its Distinctive Protease-Trapping Mechanism. *Mol. Cell. Proteomics* **2021**, *20*, No. 100090.
(37) Vilstrup, J.; Simonsen, A.; Birkefeldt, T.; Strandbygard, D.; Lyngso, J.; Pedersen, J. S.; Thirup, S. Crystal and solution structures of fragments of the human leucocyte common antigen-related protein. *Acta Crystallogr., Sect. D: Struct. Biol.* **2020**, *76*, 406−417.
(38) Steiner, E. M.; Lyngsø, J.; Guy, J. E.; Bourenkov, G.; Lindqvist, Y.; Schneider, T. R.; Pedersen, J. S.; Schneider, G.; Schnell, R. The structure of the N-terminal module of the cell wall hydrolase RipA and its role in regulating catalytic activity. *Proteins* **2018**, *86*, 912−923.
(39) Larsen, A. H.; Pedersen, J. S.; Arleth, L. Assessment of structure factors for analysis of small-angle scattering data from desired or undesired aggregates. *J. Appl. Crystallogr.* **2020**, *53*, 991−1005.
(40) Kotlarchyk, M.; Chen, S. H. Analysis of small angle neutron scattering spectra from polydisperse interacting colloids. *J. Chem. Phys.* **1983**, *79*, 2461−2469.
(41) Debye, P. Zerstreuung von Röntgenstrahlen. *Ann. Phys.* **1915**, *351*, 809−823.
(42) Sreerama, N.; Woody, R. W. Estimation of protein secondary structure from circular dichroism spectra: comparison of CONTIN SELCON, and CDSSTR methods with an expanded reference set. *Anal. Biochem.* **2000**, *287*, 252−260.
(43) Johnson, W. C. Analyzing protein circular dichroism spectra for accurate secondary structures. *Proteins: Struct., Funct., Bioinformatics* **1999**, *35*, 307−312.
(44) Sreerama, N.; Venyaminov, S. Y.; Woody, R. W. Estimation of protein secondary structure from circular dichroism spectra: inclusion of denatured proteins with native proteins in the analysis. *Anal. Biochem.* **2000**, *287*, 243−251.
(45) Frishman, D.; Argos, P. Knowledge-based protein secondary structure assignment. *Proteins* **1995**, *23*, 566−579.
(46) Dickson, M. A.; Hahn, W. C.; Ino, Y.; Ronfard, V.; Wu, J. Y.; Weinberg, R. A.; Louis, D. N.; Li, F. P.; Rheinwald, J. G. Human keratinocytes that express hTERT and also bypass a p16(INK4a)-enforced mechanism that limits life span become immortal yet retain normal growth and differentiation characteristics. *Mol. Cell. Biol.* **2000**, *20*, 1436−1447.
(47) Rappsilber, J.; Ishihama, Y.; Mann, M. Stop and Go Extraction Tips for Matrix-Assisted Laser Desorption/Ionization, Nanoelectrospray, and LC/MS Sample Pretreatment in Proteomics. *Anal. Chem.* **2003**, *75*, 663−670.
(48) Eden, E.; Navon, R.; Steinfeld, I.; Lipson, D.; Yakhini, Z. GOrilla: a tool for discovery and visualization of enriched GO terms in ranked gene lists. *BMC Bioinformatics* **2009**, *10*, 48.
(49) Mortensen, K.; Pedersen, J. S. Structural study on the micelle formation of poly(ethylene oxide)-poly(propylene oxide)-poly(ethylene oxide) triblock copolymer in aqueous solution. *Macromolecules* **1993**, *26*, 805−812.
(50) Kikhney, A. G.; Svergun, D. I. A practical guide to small angle X-ray scattering (SAXS) of flexible and intrinsically disordered proteins. *FEBS Lett.* **2015**, *589*, 2570−2577.
(51) Kohn, J. E.; Millett, I. S.; Jacob, J.; Zagrovic, B.; Dillon, T. M.; Cingel, N.; Dothager, R. S.; Seifert, S.; Thiyagarajan, P.; Sosnick, T. R.; Hasan, M. Z.; Pande, V. S.; Ruczinski, I.; Doniach, S.; Plaxco, K. W. Random-coil behavior and the dimensions of chemically unfolded proteins. *Proc. Natl. Acad. Sci. U. S. A.* **2004**, *101*, 12491−12496.
(52) Smilgies, D. M.; Folta-Stogniew, E. Molecular weight-gyration radius relation of globular proteins: a comparison of light scattering, small-angle X-ray scattering and structure-based data. *J. Appl. Crystallogr.* **2015**, *48*, 1604−1606.
(53) Tria, G.; Mertens, H. D.; Kachala, M.; Svergun, D. I. Advanced ensemble modelling of flexible macromolecules using X-ray solution scattering. *IUCrJ* **2015**, *2*, 207−217.
(54) Wittig, I.; Schägger, H. Native electrophoretic techniques to identify protein−protein interactions. *Proteomics* **2009**, *9*, 5214−5223.
(55) García-Castellanos, R.; Nielsen, N. S.; Runager, K.; Thøgersen, I. B.; Lukassen, M. V.; Poulsen, E. T.; Goulas, T.; Enghild, J. J.; Gomis-Rüth, F. X. Structural and Functional Implications of Human Transforming Growth Factor *β*-Induced Protein, TGFBIp, in Corneal Dystrophies. *Structure* **2017**, *25*, 1740−1750.
(56) Uversky, V. N. Dancing Protein Clouds: The Strange Biology and Chaotic Physics of Intrinsically Disordered Proteins. *J. Biol. Chem.* **2016**, *291*, 6681−6688.
(57) Hoersch, S.; Andrade-Navarro, M. A. Periostin shows increased evolutionary plasticity in its alternatively spliced region. *BMC Evolution. Biol.* **2010**, *10*, 30.
(58) Mishra, S. K.; Wheeler, J. J.; Pitake, S.; Ding, H.; Jiang, C.; Fukuyama, T.; Paps, J. S.; Ralph, P.; Coyne, J.; Parkington, M.; DeBrecht, J.; Ehrhardt-Humbert, L. C.; Cruse, G. P.; Bäumer, W.; Ji, R. R.; Ko, M. C.; Olivry, T. Periostin Activation of Integrin Receptors on Sensory Neurons Induces Allergic Itch. *Cell Rep.* **2020**, *31*, 107472.
(59) Hein, M. Y.; Hubner, N. C.; Poser, I.; Cox, J.; Nagaraj, N.; Toyoda, Y.; Gak, I. A.; Weisswange, I.; Mansfeld, J.; Buchholz, F.; Hyman, A. A.; Mann, M. A Human Interactome in Three Quantitative Dimensions Organized by Stoichiometries and Abundances. *Cell* **2015**, *163*, 712−723.
(60) Tumbarello, D. A.; Temple, J.; Brenton, J. D. ß3 integrin modulates transforming growth factor beta induced (TGFBI) function and paclitaxel response in ovarian cancer cells. *Mol. Cancer* **2012**, *11*, 36.
(61) Nielsen, N. S.; Poulsen, E. T.; Lukassen, M. V.; Chao Shern, C.; Mogensen, E. H.; Weberskov, C. E.; DeDionisio, L.; Schauser, L.; Moore, T. C. B.; Otzen, D. E.; Hjortdal, J.; Enghild, J. J. Biochemical mechanisms of aggregation in TGFBI-linked corneal dystrophies. *Prog. Ret. Eye Res.* **2020**, *77*, No. 100843.
(62) Kawahara, R.; Granato, D. C.; Yokoo, S.; Domingues, R. R.; Trindade, D. M.; Paes Leme, A. F. Mass spectrometry-based proteomics revealed Glypican-1 as a novel ADAM17 substrate. *J. Proteomics* **2017**, *151*, 53−65.

https://doi.org/10.1021/acs.biochem.3c00176
Biochemistry 2023, 62, 2803−2815

(63) Ben-Nissan, G.; Katzir, N.; Füzesi-Levi, M. G.; Sharon, M. Biology of the Extracellular Proteasome. *Biomolecules* **2022**, *12*, 619.
(64) Broome, A.-M.; Ryan, D.; Eckert, R. L. S100 Protein Subcellular Localization During Epidermal Differentiation and Psoriasis. *J. Histochem. Cytochem.* **2003**, *51*, 675−685.
(65) Gläser, R.; Meyer-Hoffert, U.; Harder, J.; Cordes, J.; Wittersheim, M.; Kobliakova, J.; Fölster-Holst, R.; Proksch, E.; Schröder, J. M.; Schwarz, T. The antimicrobial protein psoriasin (S100A7) is upregulated in atopic dermatitis and after experimental skin barrier disruption. *J. Investig. Dermatol.* **2009**, *129*, 641−649.
(66) Wood, S. H.; Clements, D. N.; Ollier, W. E.; Nuttall, T.; McEwan, N. A.; Carter, S. D. Gene expression in canine atopic dermatitis and correlation with clinical severity scores. *J. Dermatol. Sci.* **2009**, *55*, 27−33.
(67) Jin, S.; Park, C. O.; Shin, J. U.; Noh, J. Y.; Lee, Y. S.; Lee, N. R.; Kim, H. R.; Noh, S.; Lee, Y.; Lee, J. H.; Lee, K. H. DAMP molecules S100A9 and S100A8 activated by IL-17A and house-dust mites are increased in atopic dermatitis. *Exp. Dermatol.* **2014**, *23*, 938−941.
(68) Tomas, D.; Vucić, M.; Situm, M.; Kruslin, B. The expression of syndecan-1 in psoriatic epidermis. *Arch. Dermatol. Res.* **2008**, *300*, 393−395.
(69) Nakao, M.; Sugaya, M.; Takahashi, N.; Otobe, S.; Nakajima, R.; Oka, T.; Kabasawa, M.; Suga, H.; Morimura, S.; Miyagaki, T.; Fujita, H.; Asano, Y.; Sato, S. Increased syndecan-4 expression in sera and skin of patients with atopic dermatitis. *Arch. Dermatol. Res.* **2016**, *308*, 655−660.
(70) Seguchi, T.; Chang-Yi, C.; Kusuda, S.; Takahashi, M.; Aisu, K.; Tezuka, T. Decreased expression of filaggrin in atopic skin. *Arch. Dermatol. Res.* **1996**, *288*, 442−446.
(71) Kirino, M.; Kirino, Y.; Takeno, M.; Nagashima, Y.; Takahashi, K.; Kobayashi, M.; Murakami, S.; Hirasawa, T.; Ueda, A.; Aihara, M.; Ikezawa, Z.; Ishigatsubo, Y. Heme oxygenase 1 attenuates the development of atopic dermatitis-like lesions in mice: implications for human disease. *J. Allergy Clin. Immunol.* **2008**, *122*, 297.
(72) Sitko, K.; Bednarek, M.; Mantej, J.; Trzeciak, M.; Tukaj, S. Circulating heat shock protein 90 (Hsp90) and autoantibodies to Hsp90 are increased in patients with atopic dermatitis. *Cell Stress Chaperones* **2021**, *26*, 1001−1007.
(73) Bregnhøj, A.; Thuesen, K. K. H.; Emmanuel, T.; Litman, T.; Grek, C. L.; Ghatnekar, G. S.; Johansen, C.; Iversen, L. HSP90 inhibitor RGRN-305 for oral treatment of plaque-type psoriasis: efficacy, safety and biomarker results in an open-label proof-of-concept study*. *Br. J. Dermatol.* **2022**, *186*, 861−874.
(74) Aizawa, N.; Ishiuji, Y.; Tominaga, M.; Sakata, S.; Takahashi, N.; Yanaba, K.; Umezawa, Y.; Asahina, A.; Kimura, U.; Suga, Y.; Takamori, K.; Nakagawa, H. Relationship between the Degrees of Itch and Serum Lipocalin-2 Levels in Patients with Psoriasis. *J. Immunol. Res.* **2019**, *2019*, No. 8171373.
(75) Imai, Y. Interleukin-33 in atopic dermatitis. *J. Dermatol. Sci.* **2019**, *96*, 2−7.
(76) Kim, E. Y.; Dryer, S. E. RAGE and $\alpha V\beta 3$-integrin are essential for suPAR signaling in podocytes. *Biochim. Biophys. Acta, Mol. Basis Dis.* **2021**, *1867*, No. 166186.
(77) Lei, H.; Li, X.; Jing, B.; Xu, H.; Wu, Y. Human S100A7 Induces Mature Interleukin1α Expression by RAGE-p38 MAPK-Calpain1 Pathway in Psoriasis. *PLoS One* **2017**, *12*, No. e0169788.

https://doi.org/10.1021/acs.biochem.3c00176
Biochemistry 2023, 62, 2803−2815